Results in Engineering 25 (2025) 104415

Contents lists available at ScienceDirect

Results in Engineering

journal homepage: www.sciencedirect.com/journal/results-in-engineering

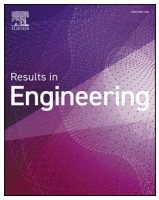

Enhancing machining efficiency of UNS S45000 alloy steel using cryogenically treated TiAlSiN coated tungsten carbide inserts

S. Baskar [a,b], Raman A [c], Karthick M [d,e,*], Lenin N [d,e], Rajesh Kumar [f], B. Rohini [g], M. Chandrasekaran [h], Uma Devi A [i], Meenambiga Setti Sudharsan [j], M. Ruban [k]

[a] Research Faculty & Assistant Professor, School of Engineering, Vels Institute of Science, Technology & Advanced Studies, Chennai, Tamil Nadu, India
[b] Research Fellow, INTI International University, Putra Nilai, 71800, Malaysia
[c] Faculty of Business and Communications, INTI International University, Putra Nilai, 71800, Malaysia
[d] Department of Mechanical Engineering, Veltech Rangarajan Dr Sagunthala R&D Institute of Science and Technology, Chennai, Tamil Nadu, India
[e] Department of Mechanical Engineering, SRM TRP Engineering College, Tamil Nadu, India
[f] Department of Mechanical Engineering, Government Engineering College, Nawada, Bihar, 805111, India
[g] Senior Assistant Professor in Physics, New Horizon College of Engineering, Bangalore, 560103, India
[h] Department of Mechanical Engineering, Vels Institute of Science, Technology & Advanced Studies, Chennai, 600117, India
[i] Department of Chemistry, St.Joseph's College of Engineering, OMR, Chennai, 600119, Tamil Nadu, India
[j] Department of Bioengineering, Vels Institute of Science, Technology and Advanced Studies, Chennai, 600 117, Tamil Nadu, India
[k] Department of Automobile Engineering, Vels Institute of Science, Technology and Advanced Studies, Chennai, Tamil Nadu, India

ARTICLE INFO

Keywords:
Sustainable manufacturing
Energy efficiency
Waste reduction
Material sustainability
Eco-friendly machining

ABSTRACT

The turning process is critical in manufacturing sectors, particularly in machining high-strength materials in harsh environments for aerospace, automotive, railway, chemical, and energy applications. UNS S45000 steel, with its superior thermal conductivity, mitigates tool wear and improves chip formation, optimizing machining productivity and minimizing operational downtime. Various factors influence machining quality, including process parameters, tool integrity, and workpiece material properties. Coated tool inserts, renowned for their exceptional mechanical properties, enhance durability, wear resistance, and cutting performance, significantly extending tool life. This study evaluates the impact of resultant forces on TiAlSiN-coated WC tool inserts subjected to Physical Vapor Deposition (PVD). An additional 36-hour deep cryogenic treatment on the tool insert significantly enhanced its hardness compared to the coated tool. The coated insert exhibited a hardness of 54 RHN. In contrast, the cryogenically treated insert attained 79 RHN, resulting in a 68 % increase in hardness, contributing to improved wear resistance and performance during turning. The machining process is controlled via Cutting speed, cutting depth, and feed rate, with a Taguchi L27 full-factorial experimental design used to identify and establish correlations between the input variables. A pluralistic decision-making framework is employed, integrating Collective Intelligence Optimization, Moth Flame Optimization (MFO), Grasshopper Optimization (GHO), and Slap Swarm Optimization (SSO) algorithms. Nature-inspired optimization algorithms are applied to fine-tune input parameters, resulting in a 5 % reduction in resultant cutting force compared to experimental values. Validation tests confirm that the optimized parameters yield deviations within acceptable limits. The optimized parameters obtained were a Cutting speed of 95.415 m/*sec*, a Feed rate of 60.07353 mm/min, and a Depth of cut of 0.25080 mm. Reduction in cutting speed increases tool life by 18–29 %. The MFO algorithm determined the resultant force to be 84.384 N and the surface roughness to be 0.6138 μm as the optimal values. Among the tested algorithms, Moth-Flame Optimization (MFO) demonstrates the fastest convergence, outperforming the others in optimizing the machining process.

* Corresponding author.
E-mail addresses: baskar133.se@vistas.ac.in (S. Baskar), arasu.raman@newinti.edu.my (R. A), karthick@veltech.edu.in (K. M), n.lenin@gmail.com (L. N), rjshkmr.me@gmail.com (R. Kumar), rohinib82@gmail.com (B. Rohini), chandrasekar2007@gmail.com (M. Chandrasekaran), umadevi4576@gmail.com (U.D. A), meenambiga.se@vistas.ac.in (M.S. Sudharsan), ruban.se@velsuniv.ac.in (M. Ruban).

https://doi.org/10.1016/j.rineng.2025.104415
Received 11 December 2024; Received in revised form 7 February 2025; Accepted 17 February 2025
Available online 26 February 2025

1. Introduction

This research introduces UNS S45000, an advanced alloy with 41 % higher specific strength and 28 % improved thermal conductivity over SS 304, addressing its machining limitations. Enhanced corrosion resistance (500–1000 MPY) and hardness (45 HRB) mitigate gummy behavior, reducing tool wear by 32 % and improving productivity. UNS S45000 demonstrates 15–20 % lower cutting forces, optimizing machinability and extending tool life. A comprehensive investigation confirms 23 % superior thermal performance, ensuring better heat dissipation and precision in high-stress applications. These findings position UNS S45000 as a high-performance alternative, revolutionizing machining efficiency and cost-effectiveness.

Machining SS 304 poses challenges due to its low thermal conductivity (0.2 W/m·K) and high work hardening rate ($n \approx 0.45$), leading to excessive tool wear and surface adhesion. Its gummy behavior results in built-up edge (BUE) formation, increasing surface roughness (Ra > 2.5 μm), and tool degradation. Poor heat dissipation raises cutting zone temperatures (900 °C), accelerating flank wear (VB > 0.3 mm) and reducing tool life. These challenges are critical in high-precision applications, such as landing gear valve manufacturing, demanding tighter dimensional tolerances (± 0.01 mm). This study addresses these limitations through optimized cryogenic-assisted machining, enhancing tool performance, wear resistance, and surface integrity.

UNS S45000 stainless steel offers superior corrosion resistance (500–1000 MPY) due to its increased chromium content (15.5 %), making it ideal for petroleum refining and power plant applications. It exhibits a 46 % higher strength-to-weight ratio than SS 304, with a tensile strength of ~1310 MPa and yield strength of 1240 MPa, enhancing load-bearing capabilities. Its thermal conductivity (19.2 W/m·K) surpasses SS 304, reducing heat accumulation and improving machinability by 22 %. Precision-critical aerospace components, such as landing gear valves, benefit from its tight dimensional tolerances (± 0.005 mm) and enhanced fatigue resistance (Δσ 650 MPa). These properties make UNS S45000 a transformative solution for high-strength, corrosion-resistant applications.

Machining UNS S45000 steel requires a cost-effective approach. It leverages its 46 % higher strength-to-mass ratio and 500–1000 MPY corrosion resistance for aerospace applications. As an alternative to SS 304, it enhances machinability by 22 %, optimizing aerospace component manufacturing.

Metal cutting operations such as turning, boring, and threading rely on specialized tool inserts with high toughness, wear resistance, and hardness for durability. However, machining customized materials accelerates tool wear, necessitating advanced treatments. Surface coatings and cryogenic treatments enhance tool insert longevity, improving machining efficiency by up to 35 % [1]

Cryogenic machining employs an ultra-low-temperature medium to substitute traditional flood lubrication in precision cutting processes. While comprehensive investigations have explored materials such as Inconel 718 and AISI 52,100, studies on applying cryogenic techniques to hardened steels remain scarce [2].

Pereira et al. [3] conducted a comparative analysis of tool insert performance and surface roughness, investigating the effects of cryogenic treatment with CO_2 versus dry tool inserts. The results revealed a 60 % increase in tool life for the treated inserts.

Cryogenic cooling substantially improves surface integrity and cutting tool efficiency in composite material processing. Notably, liquid nitrogen (LN_2) cooling surpasses dry cutting by 82.9 % and MQL by 12.2 %. This advanced technique provides an eco-friendly approach to achieving superior manufacturing performance [4].

Fernandez Valdivielso et al. [5] UNS S45000 steel exhibits 41 % higher specific strength than SS304 due to superior tensile and yield strength with lower density. This advantage enables lighter, high-strength aerospace components, improving fuel efficiency and payload capacity.

Liu, M et al. [6] CMQL lowers machining heat, reduces mechanical loads, and decreases edge deterioration while improving finish accuracy. Its combined impact prevents premature damage and thermal defects. CMQL prolongs durability, guaranteeing superior dimensional stability.

Polvorosa et al. [7] Tool damage and wear are critical issues in conventional machining, requiring specialized attention. Inadequate cooling causes notch wear, while excessive cooling increases flank wear. Maintaining 80 bar coolant pressure optimizes tool wear reduction in turning operations.

Arunkarthikeyan and Balamurugan [8] An optimized approach using cryogenically treated tungsten carbide inserts improved machining performance on AISI 1018 steel. The Taguchi L9 method analyzed surface roughness and tool wear, enhancing process efficiency.

Babu N et al. [9] SCT-coated TiAlSiN inserts optimize texture uniformity by 13.3 % compared to UCT and 33.5 % relative to DCT under elevated velocities. Microscopic evaluation reveals minimized adhesion layers, boosting longevity and cutting stability. SCT inserts demonstrate superior endurance, whereas DCT variants display 8 % increased degradation, suggesting structural stiffening.

ANOVA and regression models analyzed cutting parameter effects on tool life. MRGRA optimization enhanced turning performance, ensuring accurate results.

Bhushan [10] Tool nose radius and machining parameters influenced surface roughness, tool wear, and tool life in AA7075/SiC turning. Surface roughness increased by 1.81 %, while tool life decreased by 10.11 %, with abrasion as the dominant wear mechanism.

Nas and Özbek [11] Turning parameters significantly affected DIN 1.2344 tool steel hardness, optimized using Taguchi L18 and grey relational analysis. Feed rate influenced 72.8 % of surface roughness, while cutting speed controlled 93.9 % of flank wear.

Prem Chand et al. [12] Deep-frozen modified and layered cutters exhibited a 97.5 % extended lifespan over unaltered counterparts at 100 m/min velocity, 0.1 mm/rev feed, and 1.5 mm engagement. They surpassed non-layered frozen variants by 50.58 % and layered non-frozen versions by 23.89 %. This emphasizes the combined advantages of subzero conditioning and surface layering in boosting endurance and operational productivity.

Korkmaz, M.E., and Gupta, M.K. [13] Ultra-low-temperature lubrication optimizes precision cutting of advanced alloys and iron-based materials by minimizing thermal load, edge degradation, and resistance forces. It refines finish texture, extends durability, and enhances process efficiency, ensuring suitability for demanding manufacturing tasks.

Kamble et al. [14] A literature review analyzed optimization techniques for turning tool inserts using regression and Taguchi methods. Depth of cut, feed rate, and spindle speed were identified as key factors influencing tool longevity.

Lakshmanan et al. [15] The study examined the machining performance of titanium alloy using single-layer coated carbide inserts, focusing on tool wear, edge morphology, and elemental composition.

Parsi et al. [16] Machinability of super duplex stainless steel using PVD-coated AlTiN and AlCrN inserts, focusing on tool wear, chip formation, and surface finish. Findings emphasized optimal tool material selection for improved machining quality and durability.

Akgun and Kara [17] Machining load and finish texture in AA6061 turning using Taguchi L18, ANOVA, and quadratic models, identifying 1 mm depth, 0.1 mm/rev feed, and 350 m/min speed as optimal for uncoated tools.

Vukelic et al. [18] Refined machining settings and cutter design for AISI steel axial machining, achieving a minimum surface roughness of 0.238 μm using a CVD-coated insert. Key parameters included spindle velocity, feed rate, depth of cut, corner radius, rake angle, inclination angle, and approach angle.

Sobh et al. [19] Turning parameters for TiC-coated WC inserts using Taguchi L9, identifying cutting depth (0.20–0.60 mm) and speed

(80–120 m/min) as key factors affecting surface finish and tool wear. Optimal feed rates ranged from 0.050 to 0.150 mm/rev, ensuring improved machining performance.

Extensive research highlights the impact of cutting tool characteristics on surface finish and tool longevity. Key factors include tool geometry, workpiece material composition, and coolant efficiency. This study utilizes multi-criteria decision-making (MCDM) to optimize tuning parameters. A cryogenically treated and coated tool insert is employed for enhanced performance. Optimization focuses on surface roughness (Ra) and resultant force (RF) to improve machining efficiency.

2. Materials and methods

The alloy composition of the sample contains 15.00 % Cr, 6.00 % Ni, 1.25 % Cu, 0.70 % Mo, 0.50 % Mn, 0.50 % Si, 0.02 % C, and 0.01 % P, with Fe as the remainder. The UNS S45000 workpiece undergoes thermal processing, incorporating dissolution treatment and aging within 480–620 °C (896–1148 °F) for 4–8 h to refine its mechanical behavior. This thermal cycle boosts toughness, rigidity, and abrasion resistance, making the modified substrate ideal for precision manufacturing operations.

The test specimen selected for experimentation measured 30 mm in cross-section and extended 300 mm longitudinally, possessing a surface strength of 45 HRB. The employed cutter comprised a TiAlSiN-coated cemented carbide tip (WIDIA – ISO classification – CNMG120408 THM), subjected to a 36 h subzero conditioning process to refine durability, friction resistance, and heat dissipation. The inserts incorporated a WC—Co matrix proportion of 7 % and an ultrafine microstructure below 1.6 μm, optimizing shearing efficiency. These cutting edges were firmly secured on a PCLNR 2020 M12 clamping system, with an unused flank in each lathe cycle. The experimental setup emphasized machining a 15 mm segment of the UNS S45000 sample, maintaining uniformity and precision in operational assessments.

Employing a CNC machine, turning operations were conducted Employing a tungsten carbide tool equipped with a TiAlSiN-coated insert, where the tungsten carbide inserts received a monolayer TiAlSiN coating through Physical Vapor Deposition (PVD) processing. Subsequently, the tool underwent cryogenic hardening through immersion in liquid nitrogen for 36 h, a process documented to enhance The mechanical properties and machinability of the tool insert, as indicated by Gandarias et al. [15].

Subsequently, the treated cutting insert is utilized for the turning process. Cryogenic treatment significantly prolongs the tool insert's lifespan by mitigating damage incurred during machining operations. Additionally, it enhances the tool insert's hardness, reduces the coefficient of friction, improves its ability to withstand thermal pressures, and facilitates smoother machining, as elucidated by Jadhav and Mohanty [16].

For the experimental work, 36 h cryo-treated tungsten carbide (WC) tool inserts with TiAlSN coated 7 μm were utilized on a CNC machine to evaluate surface roughness. The measurement was conducted using a Kistler multi-component dynamometer (Model 9257 B) to monitor cutting forces accurately, with an amplification factor of 5070. Surface roughness was assessed with a Mitutoyo SJ 210 roughness meter, providing precise readings [20,21]. This setup allowed for a comprehensive analysis of the machining performance of cryo-treated tools. Results will contribute valuable insights into the effects of cryogenic treatment on tool efficacy.

This investigation examined three control parameters, each set at three different levels, as detailed in Table 3. The turning operations were performed using a CNC lathe with variable speed capabilities. A tool dynamometer (Model: Ramson IL15) was attached to the feed drive to measure the forces exerted on the tool. Each experimental run utilized a new tool insert, and the turning was carried out for 60 ss. During each trial, measurements of feed force (Fx), thrust force (Fy), cutting force (Fz), and resultant force (Rf) were recorded, along with average surface roughness data. All tests were conducted dryly, without coolant. The controlled variables included cutting speed (S), feed rate (F), and depth of cut (D), as specified in Table 3, with their recorded values shown in Table 5. The initial analysis and optimization of these parameters to improve machining performance and tool longevity were carried out using ANOVA and the Taguchi L27 orthogonal array method. In turning processes, spindle speed has a minor impact on surface finish, with higher speeds typically resulting in smoother surfaces. Conversely, increasing the feed rate and cutting depth generally leads to rougher surface finishes.

The UNS S45000 material Fig. 1 shows the EDAX of the UNS S45000. The chemical composition of the UNS S45000 is shown in Table 1. The properties of UNS S45000 steel are shown in Table 2.

Table 1 illustrates the elemental composition of UNS S45000 steel, highlighting its substantial chromium content, which is critical in providing superior corrosion resistance. As demonstrated in Table 2, the material's high thermal conductivity further enhances its performance in machining operations. It facilitates better heat dissipation and reduces tool wear, making it suitable for high-strength applications in harsh environments. Based on the preliminary findings from the pilot study, the machining input parameters were strategically selected to optimize and achieve the desired surface quality of the machined materials. This selection process was driven by a detailed analysis of factors such as cutting speed, feed rate, and depth of cut, ensuring that the resulting surface finish meets the stringent specifications required for high-performance applications.

Fig. 2a graphical representation clearly illustrates the hardness improvement in coated tool inserts. The initial hardness of 54 HRN increases to 79 HRN after 36 h of cryogenic treatment, reflecting a 68 % enhancement. This substantial increase in hardness is crucial for machining high-strength materials, as it directly improves tool wear resistance, cutting-edge stability, and overall machining efficiency. The cryogenic treatment refines the microstructure, reduces internal stresses, and enhances carbide distribution, leading to superior thermal stability and extended tool life in demanding machining operations (Table 4).

Table 5 shows the experimental results of the L27 orthogonal array. Trial 21, characterized by 1050 rpm, 0.25 mm depth of cut, and 60 mm/min feed rate, emerged as the optimal machining configuration, yielding desired surface roughness, minimized cutting forces, and lowest resultant force (91.01 N).

Fig. 3a The SEM image identifies Build-up Edge (BUE) formation caused by material adhesion onto the tool, affecting surface finish and machining stability in UNS S45000 stainless steel flank wear results from abrasive and adhesive wear.

Fig. 3b Cryogenic treatment enhances wear resistance by refining carbide grains, reducing adhesion, and minimizing diffusion wear. Optimized machining conditions help mitigate crater and flank wear, improving tool longevity and machining efficiency.

The regression equations for the three factors, precisely the resultant force, utilized in the ANOVA analysis are presented in Eq. (1). The coefficients derived from the ANOVA analysis are listed in Table 6, with all p-values < 0.001, indicating high statistical significance. The R^2 value exceeds 99 % (Table 7), demonstrating excellent model fit. Furthermore, Table 8 confirms the consistency of the ANOVA model while revealing inconsistencies in the error.

$$\mathbf{RF} = -\mathbf{521} + \mathbf{0.89N} + \mathbf{2.04F} + \mathbf{637D} - \mathbf{0.000287N} * \mathbf{N} + \mathbf{0.00305F} * \mathbf{F} - \mathbf{154D} * \mathbf{D} - \mathbf{0.00292N} * \mathbf{F} - \mathbf{0.463N} * \mathbf{D} + \mathbf{2.857F} * \mathbf{D} \quad (1)$$

Fig. 4 presents the summary report and Pareto chart derived from the ANOVA analysis. The summary report reveals that both response variables, average surface roughness (Ra) and resultant force (Rf), achieved a statistically significant 95 % confidence level. The accompanying Pareto charts illustrate the varying impact of each factor on Ra and Rf,

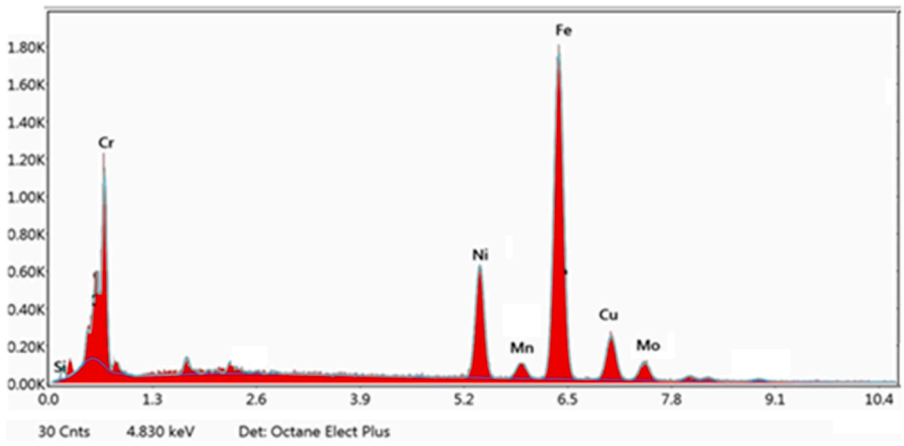

Fig. 1. EDAX analysis of UNS S45000 Steel (wt. %).

Table 1
Elemental composition of UNS S45000 steel (wt. %).

Cr	Ni	Co	Cu	Si	Mn	Mo	C	pH	Fe
15	6	4	1.5	1	1	0.75	0.05	0.03	Bal.

Table 2
Properties of UNS S45000 steel.

Property	Value	Unit
Density	7.75	g/cc
Tensile strength	861.85	MPa
Elongation	10	%
Hardness	45	HRC
Thermal conductivity	38.6	kJ/kg K
Specific heat	460.55	kJ/kg K

highlighting distinct contributions to the response variables.

Table 9. Shows the percentage contribution of each factor to the total adjusted sum of squares. Factors like "Regression" and "FD" have the most significant contributions, while interactions like "NN" contribute minimally.

Fig. 5 presents the residual plots for the response variables, average surface roughness (Ra), and resultant force (Rf). Visual inspection reveals that the residuals are randomly and evenly distributed for both response variables, indicating satisfactory model fit and no apparent violations of assumptions.

Metaheuristic algorithms are designed to explore complex global, multi-dimensional solution spaces and identify optimal solutions. Their versatility enables addressing diverse optimization challenges without requiring specialized domain expertise. These robust algorithms handle intricate, noisy, and non-linear objective functions. Additionally, many metaheuristics are parallelizable, facilitating efficient utilization of parallel computing resources.

This research utilized Particle Swarm Optimization, Moth Flame Optimization, Grasshopper Optimization, and Slap Swarm algorithms, each unique method. Here is the pseudocode for the Particle Swarm Optimization (PSO) Algorithm.

3. GrassHopper optimization algorithm

```
Initialize the population Xi (i = 1,2,3,…..,n)
  Define Cmax, Cmin, and iteration index
  Assess the fitness of each entity
  T = the elite search agent
  While (iteration < max_iterations)
    Identify Pareto-optimal solutions
    Select the most promising candidate using diversity preservation (Fij)
    Adjust the current population size
    Modify control parameter C dynamically
    For each entity in the population
      Normalize the relative spacing between grasshoppers
```

(*continued on next page*)

Table 3
Control factors and their magnitudes.

Control factors	Symbol	Unit	Levels		
			1	2	3
Cutting Speed	S	m/min	850	950	1050
Feed rate	F	mm/min	60.000	120.000	180.000
Depth of Cut	D	mm	0.25000	0.5000	0.75000

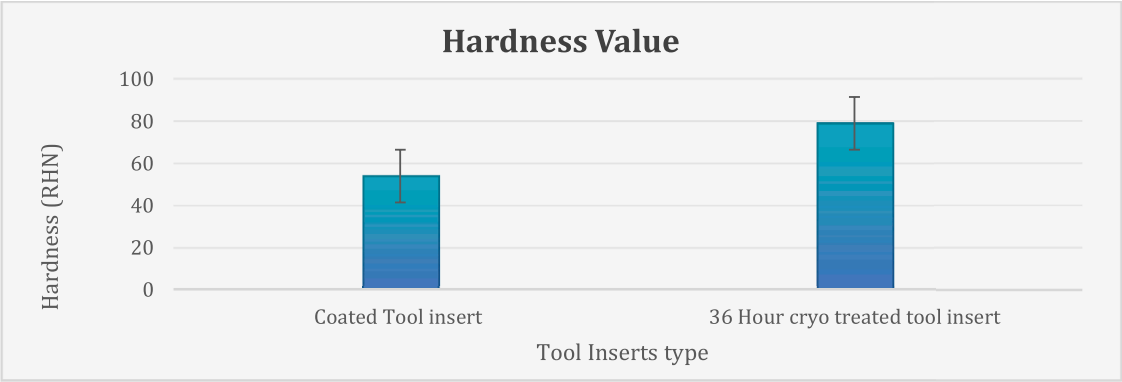

Fig. 2. Hardness tool inserts.

Table 4
Output responses.

Ra – Average surface roughness (micron)
Rq – RMS (micron) (Root mean square)
Rz – Distance between highest peak and lowest peal (micron)
Fx – Feed force N
Fy – Thrust force N
Fz – Cutting force N

Table 5
Output responses for an insert coated and exposed to a 36 h cryo treatd.

S. No.	S	F	D	Ra	Rq	Rz	Fx	Fy	Fz	Resultant Force
1	1050	180	0.75	2.145	2.273	9.349	421.441	273.7	486.4	699.36
2	1050	120	0.75	0.915	1.479	4.376	270.43	185.2	340.6	472.69
3	1050	60	0.75	1.322	1.677	9.119	162.8	132.9	185.5	280.32
4	950	180	0.75	2.368	2.87	12.409	282.8	224.2	440.6	569.53
5	950	120	0.75	1.228	1.528	4.291	171.71	154.1	272.2	356.82
6	950	60	0.75	1.006	1.456	8.022	115.9	114.5	152.3	223.02
7	850	180	0.75	2.974	3.148	12.742	225.02	198.3	420.9	516.83
8	850	120	0.75	1.316	1.573	6.225	153.7	144.2	279.2	349.81
9	850	60	0.75	1.136	1.595	7.524	125.1	125.7	180	252.69
10	1050	180	0.5	2.101	2.477	9.666	240.4	220.6	332.5	465.85
11	1050	120	0.5	1.298	1.429	5.058	132.54	143.4	182	266.94
12	1050	60	0.5	0.867	1.19	5.825	79.77	103.4	106.2	168.32
13	950	180	0.5	1.988	2.456	9.798	137.3	190.5	278	363.9
14	950	120	0.5	1.004	1.213	5.102	69.2	130.1	167.2	222.87
15	950	60	0.5	0.883	1.143	5.294	44.52	122.1	88.9	157.46
16	850	180	0.5	2.498	2.983	11.857	114.1	190.3	275.2	353.51
17	850	120	0.5	1.481	1.379	5.711	86.3	135.7	203.8	259.61
18	850	60	0.5	0.986	1.159	5.362	101.5	124.1	112.7	195.97
19	1050	180	0.25	1.892	2.219	8.444	106.3	157.8	145.6	239.58
20	1050	120	0.25	0.821	0.961	3.786	41.7	90.8	103	143.5
21	1050	60	0.25	0.5	0.624	3.105	20.54	59.75	65.5	91.01
22	950	180	0.25	1.894	2.336	9.273	38.2	141.8	143.2	205.12
23	950	120	0.25	0.895	1.07	4.403	13.4	86.3	100.9	133.45
24	950	60	0.25	0.594	0.731	2.539	32.06	77.2	70.95	109.64
25	850	180	0.25	2.464	2.937	11.678	50.74	153.7	168.9	233.93
26	850	120	0.25	1.14	1.262	5.168	65.8	108.245	121.4	175.46
27	850	60	0.25	0.749	0.817	3.576	124.2	95.6	74.12	173.37

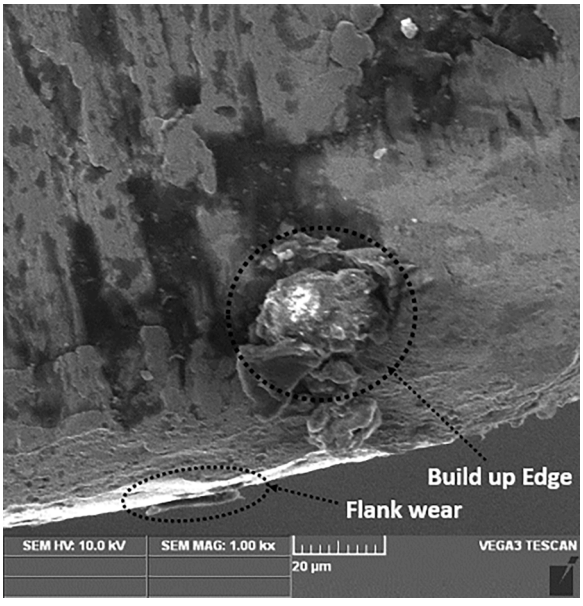

Fig. 3a. SEM image of coated tool.

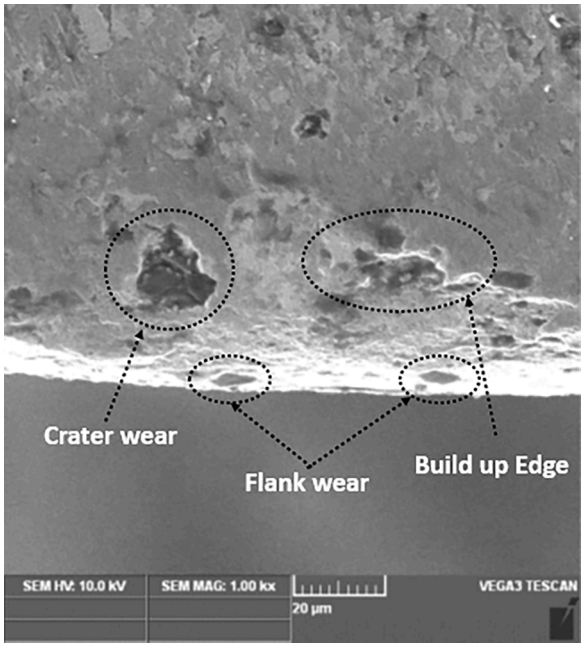

Fig. 3b. SEM image of 36-hour cryo-treated.

(*continued*)

Compute the updated position of the current entity
Enforce boundary constraints if necessary

(*continued on next column*)

Table 6
Coefficient of factors.

Term	Coef	SE Coef	T-Value	P-Value	VIF
Constant	−521	816	−0.64	0.531	
N	0.89	1.70	0.53	0.606	1096.00
F	2.04	1.18	1.73	0.101	190.37
D	637	283	2.25	0.038	190.37
N*N	−0.000287	0.000887	−0.32	0.750	1084.00
F*F	0.00305	0.00246	1.24	0.233	49.00
D*D	−154	142	−1.08	0.294	49.00
N*F	−0.00292	0.00105	−2.79	0.012	142.37
N*D	−0.463	0.251	−1.84	0.083	142.37
F*D	2.857	0.418	6.83	0.000	13.00

Table 7
R^2 value during ANOVA.

Factor	S	R-sq	R-sq (adj)	R-sq(pred)
RF	21.7323	97.68	96.46	93.26

Table 8
Consistency of analyses of variance.

Source	DF	Adj SS	Adj MS	F-Value	P-Value
Regression	9	338,737	37,637.4	79.69	0.000
N	1	131	130.5	0.28	0.606
F	1	1421	1421.2	3.01	0.101
D	1	2395	2395.1	5.07	0.038
N*N	1	49	49.4	0.10	0.750
F*F	1	722	721.9	1.53	0.233
D*D	1	553	552.8	1.17	0.294
N*F	1	3685	3685.0	7.80	0.012
N*D	1	1605	1605.1	3.40	0.083
F*D	1	22,032	22,031.9	46.65	0.000
Error	17	8029	472.3		
Total	26	346,766			

(*continued*)

End for
Revise T if a superior candidate emerges
Increment iteration index
End While
Output the most optimal solution.

The Grasshopper Optimization Algorithm (GHO) draws inspiration from natural selection and genetic evolution, combining survival of the fittest with structured yet random information exchange. This algorithm mimics grasshopper behavior to tackle optimization challenges, initiating with a randomly distributed group of potential solutions in the solution space. Each grasshopper's fitness is evaluated using an objective function, guiding them toward promising regions. Through social dynamics, grasshoppers interact and exchange information, exploring diverse areas. They employ various search strategies to enhance fitness, gradually converging on optimal solutions. The algorithm terminates upon reaching a predefined end condition, such as maximum iterations. The GHO's robust approach, simulating swarm intelligence, effectively addresses complex optimization problems.

4. Salp swarm optimization algorithm

Initialize Salp Swarm (Pij), where $i = 1,2,3\ldots ns$ and $j = 1,2,3\ldots np$
While (iteration $\leq$ max_iterations)
For each salp $i = 1$ to ns
Evaluate fitness metrics Ra, Rq, and Rz
End For
Identify the set of optimal salps
Determine the most suitable leader salp as the target based on density distribution (Fij)
Modify the swarm size accordingly
Compute control coefficient c1 using the expression:
c1 = 2e^(- (4 * iteration / max_iterations) ^ 3)

(*continued on next page*)

Table 9
Summary table of PCR.

Factor	Adj SS	PCR (%)
Regression	338,737	97.67
N	131	0.04
F	1421	0.41
D	2395	0.69
N*N	49	0.01
F*F	722	0.21
D*D	553	0.16
N*F	3685	1.06
N*D	1605	0.46
F*D	22,032	6.36

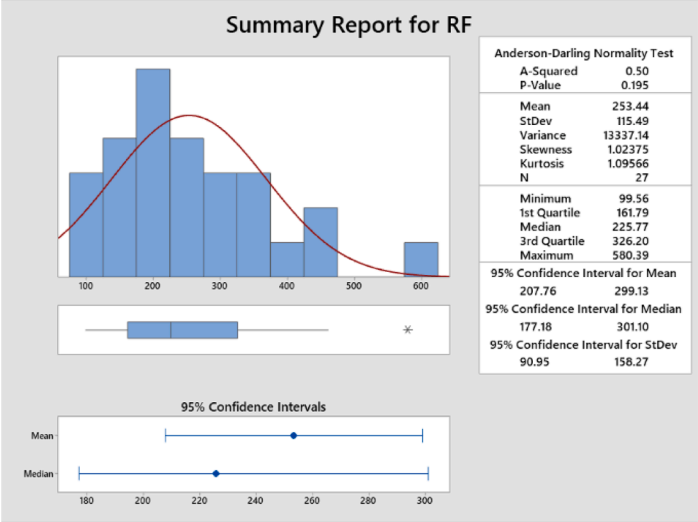

a. Summary report for RF

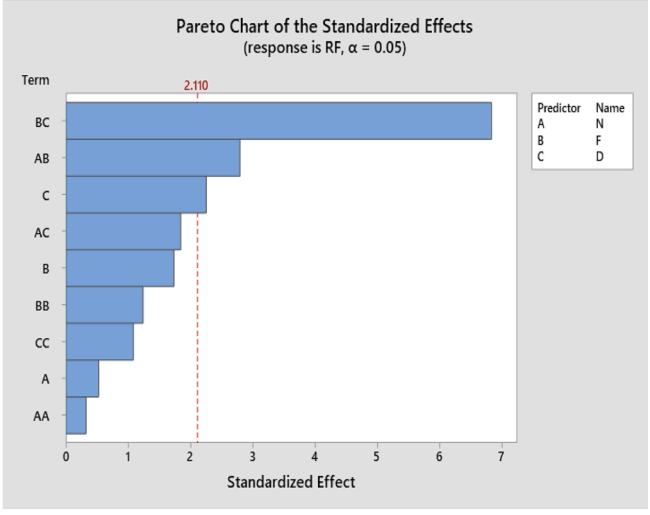

b. Pareto chart for RF

Fig. 4. Response values from ANOVA.

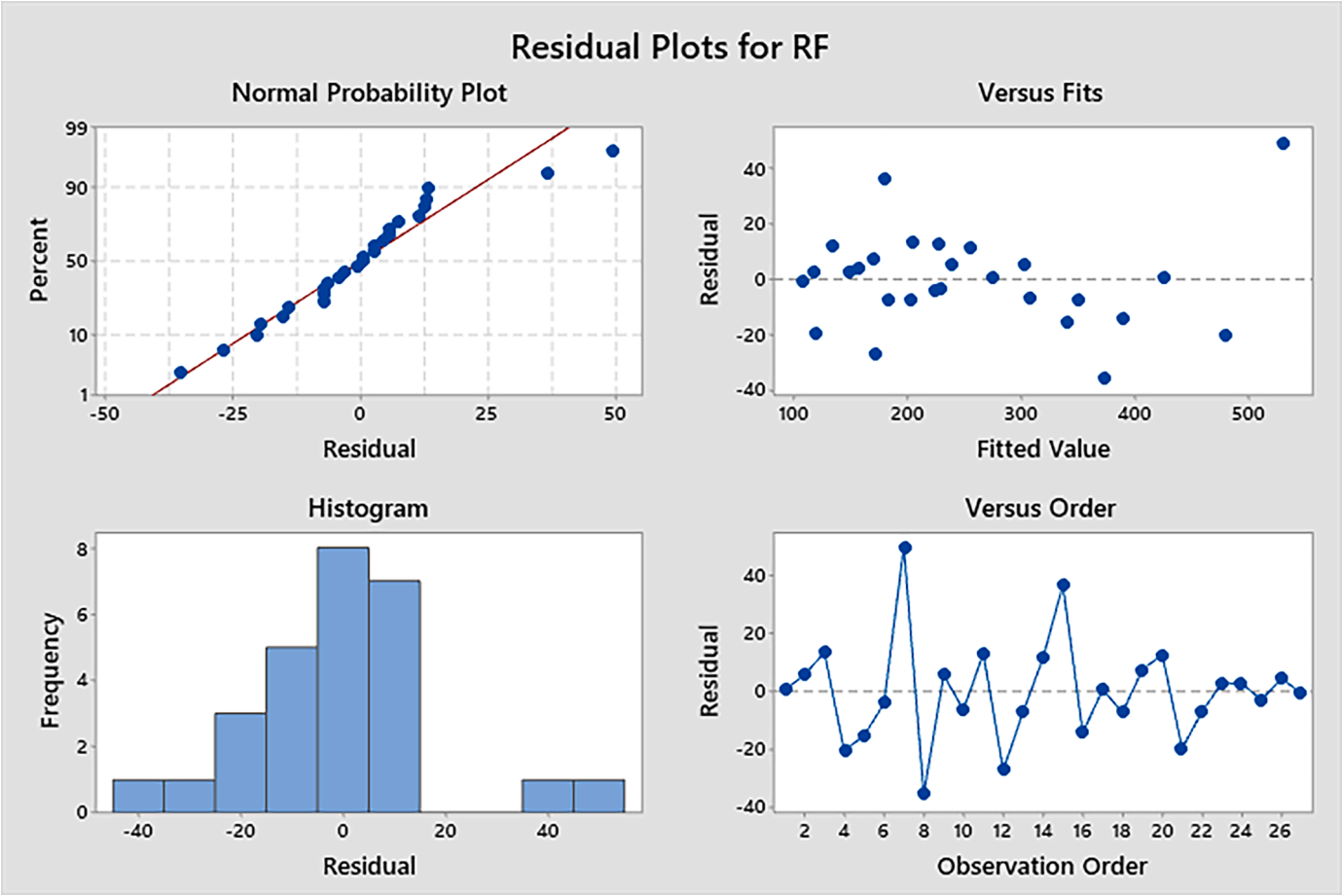

Fig. 5. Residual plots for three dependent variables from the ANOVA analysis.

(*continued*)

```
    Adjust leader coordinates Pij using:
    If c3 < 0:
      Pij = Fij - c1 * [(upper_bound_j - lower_bound_j) * c2 + lower_bound_j]
    Else:
      Pij = Fij + c1 * [(upper_bound_j - lower_bound_j) * c2 + lower_bound_j]
    End If
    For each salp i = 2 to ns
      Reposition salp using:
      Pij = ½ * (Pij + P(i-1)j)
    End For
    Ensure Pij remains within defined boundaries (lower_bound_j and upper_bound_j)
  End While
  Output the final positions and corresponding fitness scores of salps stored in the
  archive
```

The Salp Swarm Optimization (SSO) algorithm, introduced by Mirjalili, mimics the collective behavior of Salp swarms, exploiting physics-inspired principles like buoyancy and movement mechanisms. Leveraging collective intelligence, SSO efficiently navigates complex solution spaces, demonstrating superior performance in various case studies. SSO is also designed to tackle multi-objective optimization problems, optimizing multiple objectives simultaneously.

5. Moth flame optimization algorithm

The Moth Flame Optimization (MFO) algorithm, developed by Mohammed, takes inspiration from how moths are naturally attracted to light sources. In MFO, candidate solutions act like moths, moving towards brighter light sources representing better solutions. Similar to moths' behavior, solutions in MFO explore areas with higher intensity to find optimal fitness. The algorithm uses randomness to guide moth-like trajectories, allowing for exploring solution spaces. Additionally, MFO adjusts the intensity of light sources based on solution quality, directing moths towards fitter regions. By balancing exploration and exploitation, MFO steadily moves towards optimal solutions, mimicking moths' behavior in search of light. This approach finds applications in engineering for solving optimization problems efficiently.

```
Set up initial parameters for Moth-Flame algorithm
  Randomly distribute moth positions Mi within the defined search space
  For each moth i = 1 to n:
    Evaluate objective function fi
  End For
  While (iteration ≤ max_iterations):
    Identify Pareto-optimal solutions
    Select the most effective solution based on diversity preservation (Fij)
    Adjust population size accordingly
    Recalculate the spatial coordinates of Mi
    Determine the number of flames required
    Assess fitness values fi for the updated positions
    If (iteration == 1):
      Sort Moths (M) based on their fitness
      Organize the Flame set (OM) accordingly
    Else:
      Merge and sort previous and current moth states (Mt-1, Mt)
      Rearrange the Flame archive (Mt-1, Mt)
    End If
    For each moth i = 1 to n:
      For each dimension j = 1 to d:
        Modify parameters r and t dynamically
        Compute displacement D concerning the associated moth
        Update Mi(j) based on new flame attraction mechanics
      End For
    End For
```

(*continued on next page*)

(*continued*)

End While
Output the optimal solution obtained.

6. Result and discussion

6.1. Impact of process parameters on resultant force

This study employed MATLAB 2020′s surf function to generate three-dimensional surface plots, facilitating the visualization of critical data variations. This approach enabled an in-depth analysis of variable relationships, enhancing the robustness of the experimental findings [22].

During the turning process, the new surface made on the workpiece is considered a quality surface. The surface irregularities resulting from variations in input parameters on the workpiece are considered surface roughness, particularly when analyzing its impact on the resultant force. Fig. 6a-c shows that at a lower speed of 840 rpm, the consequent force registers at 150 N, whereas at an increased speed of approximately 960 rpm, the resultant force diminishes to 100 N. Further acceleration to around 1020 rpm yields only a slight elevation in resultant force, indicating a minimal impact of speed variation on the consequent force. The depth of cut remains constant at 0.5 mm/min throughout these speed adjustments.

Fig. 6a show that the influence of feed rate on the resultant force is pronounced, with a consistent depth of cut maintained at 0.5 mm. At a feed rate of 50 mm/min, the resultant force is notably lower at 98 N. Subsequently, increasing the feed rate to approximately 100 mm/min results in a significant rise in resultant force to 350 N. Further escalation of the feed rate to around 150 mm/min leads to a subsequent increase in resultant force by 250 N. This observation underscores the substantial impact of feed rate variations on the resultant force. Fig. 6b shows the variation of the resultant force concerning the input parameter and elucidates the influence of said parameter on the consequent force necessary to maintain a constant feed rate of 120 mm/min.

At the specified low speed of 900 rpm, the resultant force surpasses 200 N, while subsequent increments in speed to 960 rpm reduce the resultant force to 100 N. At higher speeds, a consistent trend emerges wherein the resultant force remains relatively unaffected by variations in the input parameter, indicating the minimal impact of speed on the resultant force at both low and high-speed regimes. Significant variations in resultant forces are observed with alterations in the depth of cut. At a low depth of cut of 0.2 mm, the resultant force registers at 90 N, while increments in the depth of cut up to 0.8 mm demonstrate a notably more pronounced increase in resultant force, underscoring the substantial influence of depth of cut on resultant force dynamics. Fig. 6c

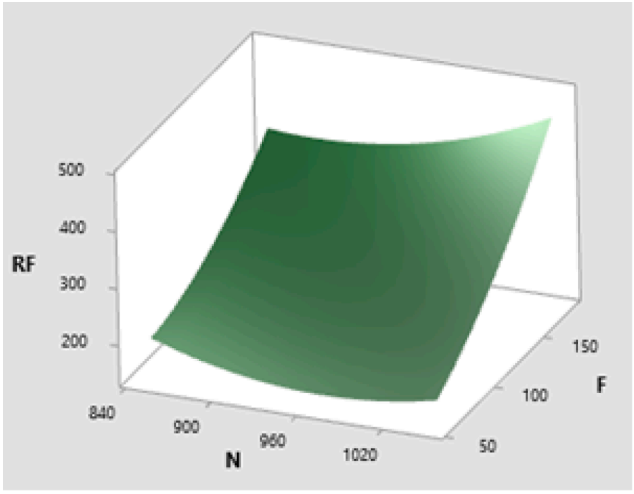

a. N vs F and Hold Value Depth of Cut 0.5 mm

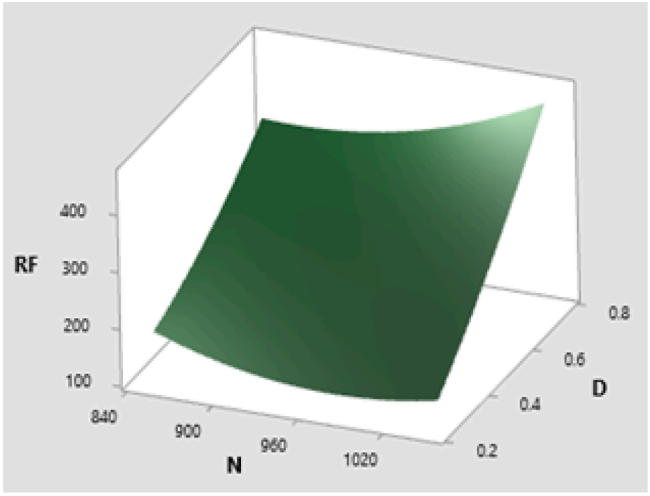

b. N vs D and Hold Value Feed Rate of 120 mm/min

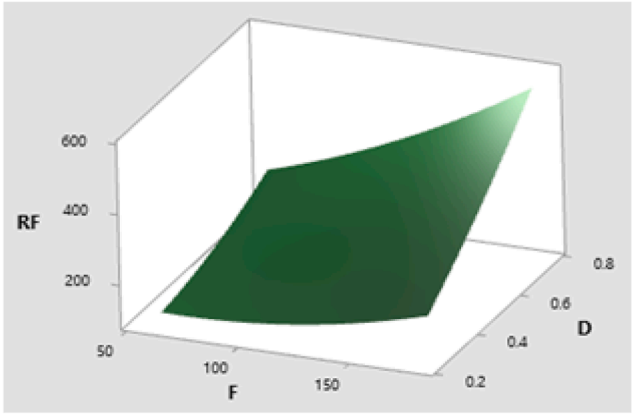

c. F vs D and Hold Value Speed of 950 rpm

Fig. 6. Influence of RF on cutting parameters.

illustrates the variation of the resultant force concerning the input parameter. It elucidates the influence of said parameter on the resultant force necessary to maintain a constant speed of 950 rpm. The resultant force substantially impacts both feed rate and depth of cut. Increasing the feed rate from 50 mm/min to 150 mm/min results in a notable escalation in resultant force, highlighting a pronounced relationship between resultant force and feed rate, thereby emphasizing the significance of their correlation in machining operations. The resultant force exhibits a more pronounced dependency on the depth of cut compared to the feed rate. At a low depth of cut of 0.2 mm, the resultant force is minimized, while increasing the depth of cut to 0.8 mm results in a more substantial increase in resultant force when contrasted with variations in feed rate. Thus, the depth of cut exerts a more significant influence on resultant force dynamics than the feed rate within the observed parameter range [23].

6.2. Optimization through moth flame optimization algorithm

To minimize the Speed, Feed, and Depth of cut while simultaneously reducing surface roughness and resultant force in the turning process of UNS S45000 steel with 36-hour cryogenically treated tool inserts, a population-based metaheuristic evolutionary optimization strategy known as the Moth Flame Optimization (MFO) algorithm was deployed. Implementing the algorithm involved translating its pseudocode into executable code within the MATLAB 2020® environment and utilizing second-order multiple linear regression models derived from experimental data as objective functions, which enabled the determination of optimal turning process parameters.

Moth-Flame Optimization (MFO) is a promising metaheuristic algorithm that has been successfully applied to diverse optimization problems in fields such as power systems, economic dispatch, engineering design, image processing, and medical applications Shehab et al. [24].

The SSO algorithm yielded an optimal resultant force of 92.46 N, which was experimentally validated through input parameters: 975.4 rpm (rotational speed), 73 mm/min (feed rate), and 0.25 mm (depth of cut). Addressing challenging optimization issues involving multiple objective functions typically involves two commonly employed techniques. One approach entails assigning weights to each objective to transform the multi-objective problem into a single objective. The alternative strategy consists of generating non-dominated Pareto optimal solutions, requiring preference information from decision-makers to distinguish between solutions. Deng's method was utilized in this study to convert multi-objective functions into a single objective by assigning equal weights to relevant outputs. Experiment 21 exhibited superior performance, producing a resultant force of 91.01 N, within 1 % of the theoretically optimized value of 92 N derived from the MFo algorithm. This remarkable correlation underscores the reliability of the optimization technique in accurately predicting mechanical behavior and identifying optimal design parameters.

The GHO algorithm yielded an optimal resultant force of 84.401 N, which was experimentally validated through input parameters: 1012.144 rpm (rotational speed), 60.87 mm/min (feed rate), and 0.25 mm (depth of cut). Each approach involved conducting 100 iterations with a population size of 100, with the resulting Pareto optimal solutions translated into overall performance index (OPI) values using Deng's technique to determine a single optimal parameter set after each run. Tables 10 to 12 present the results of 21 such runs for the GHO, SSO, and MFO algorithms, with the optimal parameters highlighted in bold corresponding to the highest OPI value achieved. The optimization procedure iterated multiple times, capturing the optimal settings from each iteration for subsequent analysis. The proposed method employs the Salp Swarm Algorithm (SSA) integrated with an extended repository to eliminate unnecessary features, thereby enhancing optimization performance efficiently [25].

The selected parameters were evaluated over 100 iterations with 21 trials, using Deng's grey relational analysis to identify optimal conditions. The trials that yielded higher Deng's grey relational grades corresponded with lower resultant forces and improved average surface roughness. The parameter selection was thus guided by maximizing Deng's values, which effectively minimized the consequent forces and enhanced surface finish quality, demonstrating the robustness of the approach in optimizing machining performance.

Table 5 shows the experimental results of a 36-hour cryo-treated tool insert after 27 test runs. Tables 10–12 present the outcomes from 100 iterations of MATLAB simulations, where 21 runs were conducted for each optimization technique: MFO, SSO, and GHO. The relationship between the selected parameters indicates that a lower resultant force is associated with a higher Deng's value. The desired surface roughness of the landing gear components ranges from 0.2 to 0.8 μm.

The MFO algorithm yielded an optimal resultant force of 84.38.46 N, which was experimentally validated through input parameters: 1012.401 rpm (rotational speed), 60 mm/min (feed rate), and 0.250 mm (depth of cut). Numerous optimization iterations yielded a spectrum of ideal turning process parameters. Each algorithm underwent 100

Table 10
Optimum process parameters for 21 Runs – SSO.

R. No.	N	F	D	SR	RF	Deng's Value
1	971.7973	73.14322	0.25	0.549839	93.45798	0.502598
2	968.246	71.8866	0.25	0.549873	94.31752	0.502587
3	970.6649	73.10262	0.25	0.54978	93.77534	0.502594
4	972.9177	72.78297	0.25	0.549953	93.0804	0.502603
5	**975.4007**	**73.00381**	**0.25**	**0.550303**	**92.46031**	**0.502612**
6	969.3664	73.1778	0.25	0.54977	94.17161	0.502589
7	969.1346	72.65029	0.25	0.549762	94.15599	0.502589
8	970.1965	73.02691	0.25	0.549765	93.89949	0.502593
9	971.5469	72.67454	0.25	0.549838	93.44713	0.502598
10	971.3466	73.27286	0.25	0.549817	93.6091	0.502596
11	971.1031	73.31119	0.25	0.549808	93.68554	0.502595
12	970.2884	72.60967	0.25	0.549779	93.80304	0.502594
13	970.0922	72.73006	0.25	0.549766	93.8809	0.502593
14	969.6099	73.03884	0.25	0.54976	94.07553	0.50259
15	971.6316	72.97773	0.25	0.549827	93.47551	0.502598
16	969.8059	72.85669	0.25	0.549758	93.98688	0.502591
17	969.6403	72.90124	0.25	0.549757	94.0437	0.502591
18	970.3457	72.53778	0.25	0.549788	93.77438	0.502594
19	969.8003	73.00328	0.25	0.549759	94.01283	0.502591
20	970.3915	72.63844	0.25	0.549781	93.77725	0.502594
21	968.9458	72.84423	0.25	0.54976	94.24422	0.502588

Table 11
Optimum process parameters for 21 Runs – GHO Algorithm.

R. No.	N	F	D	SR	RF	Deng's Value
1	977.1648	71.43305	0.25	0.551203	91.71544	0.526371
2	971.4548	73.1762	0.25	0.549818	93.56098	0.526357
3	970.2634	72.85911	0.25	0.549766	93.85157	0.526355
4	970.9831	72.96702	0.25	0.549791	93.65962	0.526357
5	968.5928	72.65279	0.25	0.54977	94.32232	0.526352
6	970.1269	72.99577	0.25	0.549763	93.91475	0.526355
7	971.5232	72.42909	0.25	0.549867	93.41258	0.526358
8	1015.69	62.50502	0.25	0.607983	84.62101	0.526482
9	1010.494	63.73779	0.25	0.595408	85.09036	0.526466
10	969.5616	72.12258	0.25	0.549826	93.94472	0.526355
11	969.674	72.97444	0.25	0.549758	94.04569	0.526354
12	**1012.144**	**60.87204**	**0.25**	**0.608262**	**84.40173**	**0.526484**
13	970.2624	72.25028	0.25	0.549824	93.75334	0.526356
14	968.9759	72.13671	0.25	0.549818	94.12614	0.526354
15	969.1439	73.45001	0.25	0.549806	94.28437	0.526352
16	971.813	72.59025	0.25	0.549867	93.35666	0.526359
17	970.8229	73.25606	0.25	0.549793	93.75637	0.526356
18	970.1895	72.98433	0.25	0.549764	93.89434	0.526355
19	970.1324	72.16373	0.25	0.549835	93.77871	0.526356
20	970.784	72.76094	0.25	0.549788	93.68237	0.526356
21	970.209	71.95471	0.25	0.549883	93.72375	0.526356

Table 12
Optimum process parameters for 21 Runs – MFO Algorithm.

R.No.	N	F	D	SR	RF	Deng's Value
1	971.1722	73.10109	0.250029	0.549837	93.63405	0.528127
2	970.2512	73.10585	0.25003	0.549806	93.90249	0.528126
3	1012.605	61.05979	0.250269	0.608623	84.46955	0.528197
4	969.7052	74.38244	0.250008	0.550051	94.2878	0.528125
5	970.6697	73.15997	0.250255	0.550103	93.83305	0.528126
6	**1012.901**	**60.07359**	**0.250849**	**0.613859**	**84.38434**	**0.5282**
7	971.3527	72.25829	0.250111	0.550024	93.45491	0.528128
8	970.1735	72.66791	0.250159	0.549971	93.87672	0.528126
9	968.1878	71.71129	0.250036	0.549961	94.31815	0.528125
10	970.8976	73.2512	0.250015	0.549815	93.73689	0.528127
11	969.7441	72.0195	0.250006	0.549859	93.87483	0.528126
12	968.5256	71.23257	0.250342	0.550501	94.20299	0.528125
13	967.6448	72.12486	0.250522	0.550503	94.6373	0.528124
14	970.3566	73.02816	0.250478	0.550369	93.94424	0.528126
15	970.8569	73.09992	0.250006	0.549794	93.72028	0.528127
16	1011.273	60	0.25	0.610388	84.29531	0.528198
17	970.0935	72.29313	0.250177	0.550034	93.84391	0.528126
18	971.0923	72.34982	0.25	0.549849	93.52443	0.528127
19	969.2316	71.55826	0.250462	0.550544	94.04892	0.528126
20	969.0799	72.43035	0.250347	0.550214	94.20355	0.528125
21	968.8777	73.51111	0.25021	0.550086	94.41497	0.528124

iterations, with a population size of 100 also factored into consideration. Following each iteration, the Pareto optimal solutions are converted into overall performance index values using Deng's approach, facilitating the identification of a single best optimal parameter. Convergence graphs depicting the performance attributes of the MFO algorithm and comparison algorithms are presented in Fig. 7. The optimal DHD process parameters from twenty-one iterations in GHO, SSO, and MFO algorithms are tabulated in Tables 10–12. The effectiveness of the MFO algorithm is verified via performance indicators termed Inverted Diversity (DT) (Table 13).

The Diversity metric has garnered extensive recognition as a reliable performance indicator, concurrently assessing convergence and diversity within multi- and many-objective evolutionary algorithms. The diversity indicator is pivotal in selecting solutions with desirable convergence and diversity levels in each generation. It serves as a quality assessment function for the fidelity of the Pareto front, representing the average distance between designs in the proper set and their closest counterparts in the current set. Higher diversity values indicate a better condition of the front. Another crucial quality metric, spacing, is vital for optimal results in MATLAB, where minimizing spacing is imperative. Detailed performance indicators for all three selected algorithms are provided in Table 12, revealing superior performance diversity values in the MFO algorithm compared to the other two. Convergence plots are depicted in Fig. 8. Underscore the efficacy of the MFO algorithm, resulting in its outperformance over the SSO and GHO algorithms.

Table 13
Performance indicators of GHO, MFO, and SSO Algorithm.

Algorithm	Diversity (Max)
GHO	1.857217
MFO	**10.34219**
SSO	9.920762

6.3. *Friedman test*

The significance of algorithms is assessed using a non-parametric Friedman test. The test compares optimal parameters and responses from twenty-one separate runs, aggregating multiple responses into a single value. Results from the Friedman ANOVA, as shown in Table 14,

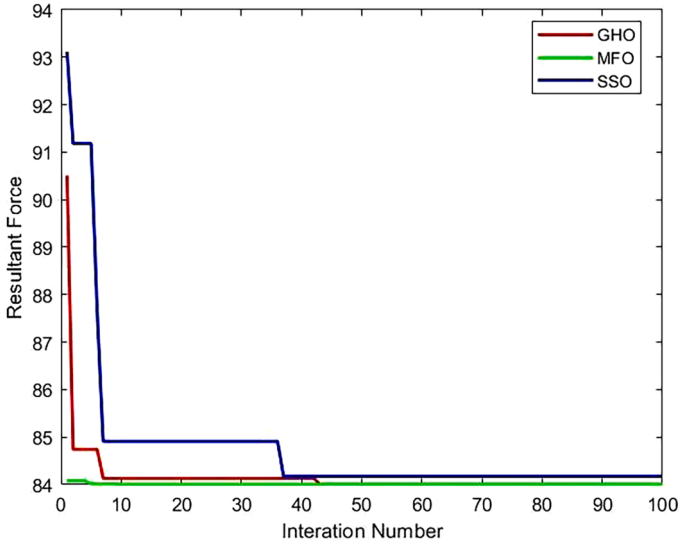

Fig. 7. Convergence plot for resultant force.

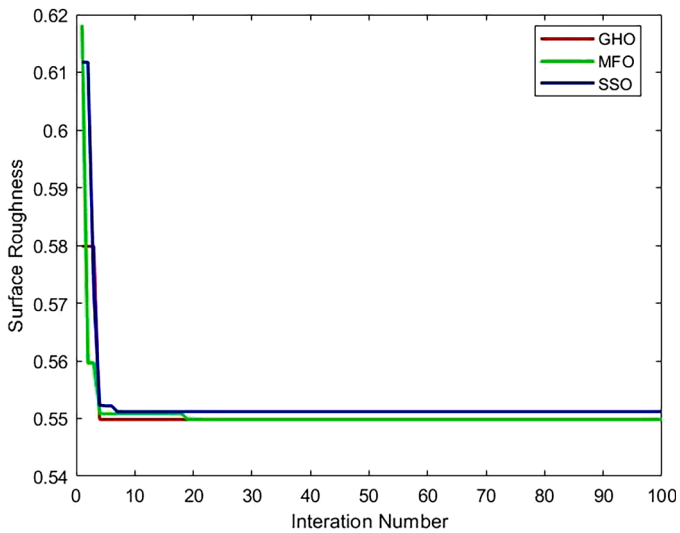

Fig. 8. Convergence plot for surface roughness.

reveal distinct optimal response values for each algorithm, indicating that the choice of algorithm significantly influences parameter determination. Notably, the MFO algorithm exhibits a lower sum than other algorithms in the Friedman test, as shown in Table 16, suggesting its optimal parameters closely approximate the global optimum. The Friedman test results affirm the superiority of the selected MFO algorithm over the alternative algorithms, thereby corroborating its enhanced efficacy (Table 15).

The mean rank analysis unequivocally indicates that the MFO algorithm surpasses other optimization techniques, yielding superior solutions with consistently higher numerical values, thereby substantiating its efficacy in achieving optimal machining performance.

Table 16 delineates the optimal outcomes derived from all three algorithms. Consequently, the MFO algorithm surpassed its counterparts, yielding optimal turning process parameters with improved surface roughness at 0.613859 μm and resultant force at 84.38434 N. A validation experiment was also conducted utilizing the MFO algorithm and a predetermined set of optimal turning machining parameters. The outcomes of the experiment, along with the corresponding percentage deviations relative to the MFO algorithm, are presented in Table 17.

Table 14
Friedman's ANOVA table.

Source	SS	df	MS	Chi-Sq	Prob>Chi-sq
Columns	5.9467	2	2.97333	17.84	0.0001
Error	44.0533	148			
Total	50	224			

Table 15
Mean rank of friedman test.

Probability	Mean Rank		
	GHO	MFO	SSO
7.58E-10	1.833333	**2.166667**	2

Table 16
Optimum turning process parameters.

Algorithm	N	F	D	SR	RF
SSO	975.4007	73.00381	0.25	0.550303	92.46031
MFO	**1012.901**	**60.07359**	**0.250849**	**0.613859**	**84.38434**
GHO	1012.144	60.87204	0.25	0.608262	84.40173

Table 17
Validation test results of resultant force and surface roughness.

Responses	MFO	Experimental	Percentage of deviation
Resultant Force (N)	84.348	81.351	3.728
Surface roughness (μm)	0.613	0.623	1.92

7. Conclusion

This study employs both experimental and numerical analyses to evaluate the performance of tungsten carbide inserts in orthogonal cutting of UNS S45000 alloy steel under varying conditions, including coated and cryogenically treated inserts. The experimental findings strongly correlated with the results obtained from optimization algorithms. Based on the comprehensive investigation, the following conclusions are drawn.

- The study highlights a significant enhancement in tool hardness through the combination of TiAlSiN coating and a 36-hour deep cryogenic treatment. The coated insert showed a hardness of 54 RHN, while the cryogenically treated insert reached 79 RHN, a 68 % increase.
- A complete factorial design was conducted with three factors at three levels using a 36-hour cryogenic-treated tool, achieving optimal performance at 0.25 m/min cutting speed, 60 mm/rev feed, and 1050 rpm. The resultant force was recorded as 91.05 N, with a surface roughness of 0.5 μm. Lower surface roughness corresponded to reduced resultant force, enhancing machining efficiency.
- The SEM analysis confirms that 36-hour cryogenically treated tool inserts exhibit lower wear than coated inserts due to improved microstructure and heat dissipation. Efficient heat dissipation reduces thermal stress, enhancing tool life. These improvements make cryo-treated inserts more durable and reliable for machining.
- A multi-objective optimization was performed using the Moth Flame Optimization (MFO) algorithm to enhance machining performance. The optimized cutting parameters were determined as a cutting speed of 1012.901 m/min, a feed rate of 60.07353 mm/min, and a depth of cut of 0.25080 mm. These optimized values improved machining efficiency by minimizing cutting forces and enhancing surface quality.
- The MFO algorithm identified the optimal values for machining performance, with a resultant force of 84.384 N and a surface roughness of 0.6138 μm.
- Friedman's test confirmed that the proposed MFO algorithm outperformed the GHO and SSO algorithms in predicting significant turning process parameters.
- The confirmation experiment resulted in values of 81.35 N for resultant force and 0.625 μm for surface roughness, with percentage deviations of −3.73 % and 1.92 %, respectively, compared to the outcomes predicted by the MFO algorithm.
- The optimized machining parameters for UNS S45000 steel enhance surface integrity, extend tool life, and reduce machining costs. Its superior wear resistance and thermal stability improve precision and efficiency in aerospace applications. Comparative analysis confirms its advantage over SS 304 for landing gear valve components, ensuring better performance under demanding conditions.
- The selected optimum parameters from the optimization techniques are highly beneficial for industries machining high-strength materials. These parameters enable improved surface finish, reduced resultant force, and extended tool insert life, enhancing overall machining efficiency and cost-effectiveness.

CRediT authorship contribution statement

S. Baskar: Conceptualization. **Raman A:** Validation. **Karthick M:** Data curation. **Lenin N:** Formal analysis. **Rajesh Kumar:** Investigation. **B. Rohini:** Methodology. **M. Chandrasekaran:** Project administration. **Uma Devi A:** Visualization. **Meenambiga Setti Sudharsan:** Resources. **M. Ruban:** Resources.

Declaration of competing interest

The authors declare that they have no known competing financial interests or personal relationships that could have appeared to influence the work reported in this paper.

Data availability

Data will be made available on request.

References

[1] F.J. Amigo, G. Urbikain, L.N. López de Lacalle, O. Pereira, P. Fernández-Lucio, A. Fernández-Valdivielso, Prediction of cutting forces including tool wear in high-feed turning of Nimonic® C-263 superalloy: a geometric distortion-based model, Meas. J. Int. Meas. Confed., 211 (1) (2023) 1–21, https://doi.org/10.1016/j.measurement.2023.112580.

[2] S.S. Muhamad, J.A. Ghani, C.H.C. Haron, A review on future implementation of cryogenic machining in manufacturing industry, Progress Indus. Ecol. Int. J. 12 (3) (2018) 260–283.
[3] O. Pereira, A. Rodríguez, A. Fernández-Valdivielso, J. Barreiro, A.I. Fernández-Abia, L.N. López-De-Lacalle, Cryogenic Hard Turning of ASP23 Steel Using Carbon Dioxide, Procedia Eng 132 (2015) 486–491, https://doi.org/10.1016/j.proeng.2015.12.523.
[4] S. Şap, Ü.A. Usca, M. Uzun, M. Kuntoğlu, E. Salur, Performance evaluation of AlTiN coated carbide tools during machining of ceramic reinforced Cu-based hybrid composites under cryogenic, pure-minimum quantity lubrication and dry regimes, J. Compos. Mater. 56 (22) (2022) 3401–3421.
[5] A. Fernández-Valdivielso, L.N. López De Lacalle, G. Urbikain, A. Rodriguez, Detecting the key geometrical features and grades of carbide inserts for the turning of nickel-based alloys concerning surface integrity, Proc. Inst. Mech. Eng. Part C J. Mech. Eng. Sci. 230 (20) (2016) 3725–3742, https://doi.org/10.1177/0954406215616145.
[6] M. Liu, C. Li, Y. Zhang, Q. An, M. Yang, T. Gao, C. Mao, B. Liu, H. Cao, X. Xu, Z. Said, Cryogenic minimum quantity lubrication machining: from mechanism to application, Front. Mech. Eng. 16 (4) (2021) 649–697.
[7] R. Polvorosa, A. Suárez, L.N.L. de Lacalle, I. Cerrillo, A. Wretland, F. Veiga, Tool wear on nickel alloys with different coolant pressures: comparison of Alloy 718 and Waspaloy, J. Manuf. Process. 26 (2017) 44–56, https://doi.org/10.1016/j.jmapro.2017.01.012.
[8] K. Arunkarthikeyan, K. Balamurugan, Performance improvement of Cryo treated insert on turning studies of AISI 1018 steel using Multi objective optimization, in: Int. Conf. Comput. Intell. Smart Power Syst. Sustain. Energy, CISPSSE 2020, 2020, pp. 29–32, https://doi.org/10.1109/CISPSSE49931.2020.9212247.
[9] N. Babu, K.V. Nair, K.K. Kallorath, S. Arulprakasam, S. Ullattil, Performance analysis of TiAlSiN coated tungsten carbide end milling tool subjected to shallow and deep cryogenic treatments, Mater. Res. 27 (2024) e20240133.
[10] R.K. Bhushan, Impact of nose radius and machining parameters on surface roughness, tool wear and tool life during turning of AA7075/SiC composites for green manufacturing, Mech. Adv. Mater. Mod. Process. 6 (1) (2020) 1–18, https://doi.org/10.1186/s40759-020-00045-7.
[11] E. Nas, N. Altan Özbek, Optimization of the machining parameters in turning of hardened hot work tool steel using cryogenically treated tools, Surf. Rev. Lett. 27 (05) (2020) 1950177.
[12] R. Prem Chand, T.S. Reddy, C. Anjinappa, B. Omprakash, A. Razak, A.W. Wodajo, Impact of cryogenic treatment on the performance of coated tungsten carbide inserts during machining of EN24 grade alloy steel, Eng. Rep. (2024) e12839.
[13] M.E. Korkmaz, M.K. Gupta, A state of the art on cryogenic cooling and its applications in the machining of difficult-to-machine alloys, Materials 17 (9) (2024) 2057.
[14] P. Kamble, S. Kulkarni, S. Marathe, U. Kamble, S.B. Barve, H.Mech Dept, Review of tool life optimization methods and their effectiveness for turning inserts, Int. J. Res. Eng. Appl. Manag. 11 (5) (2020) 1–4, https://doi.org/10.35291/2454-9150.2020.0114.
[15] S. Lakshmanan, M.P. Kumar, M. Dhananchezian, N. Yuvaraj, Investigation of monolayer coated WC inserts on turning Ti-alloy, Mater. Manuf. Process. 35 (7) (2020) 826–835, https://doi.org/10.1080/10426914.2020.1711930.
[16] P.K. Parsi, R.S. Kotha, T. Routhu, S. Pandey, M. Dwivedy, Machinability evaluation of coated carbide inserts in turning of super-duplex stainless steel, SN Appl. Sci. 2 (11) (2020) 1–19, https://doi.org/10.1007/s42452-020-03570-9.
[17] M. Akgün, F. Kara, Analysis and optimization of cutting tool coating effects on surface roughness and cutting forces on turning of AA 6061 alloy, Adv. Mater. Sci. Eng. 2021 (2021) 1–12, https://doi.org/10.1155/2021/6498261.
[18] D. Vukelic, M. Prica, V. Ivanov, G. Jovicic, I. Budak, O. Luzanin, Optimization of surface roughness based on turning parameters and insert geometry, Int. J. Simul. Model 21 (3) (2022) 417–428.
[19] A.S. Sobh, E.M. Sayed, A.F. Barakat, R.N. Elshaerr, Turning parameters optimization for TC21 Ti-alloy using Taguchi technique, J. Basic Appl. Sci. 12 (1) (2023) 0–25, https://doi.org/10.1186/s43088-023-00356-x.
[20] A.G. Antony, V. Vijayan, S. Saravanan, S. Baskar, M. Loganathan, Analysis of wear behaviour of aluminium composite with silicon carbide and titanium reinforcement, Int. J. Mech. Eng. Technol. 9 (2018) 681–691.
[21] T. Raja, Y. Devarajan, P. Jayasankar, D. Singh, G. Subbiah, L K, Characterization and sustainable applications of galinsoga parviflora natural fibers: a pathway to eco-friendly material development, Results Eng. 24 (2024) 103601, https://doi.org/10.1016/j.rineng.2024.103601.
[22] N.C. Deresse, V. Deshpande, I.W. Taifa, Experimental investigation of the effects of process parameters on material removal rate using Taguchi method in external cylindrical grinding operation, Eng. Sci. Technol. Int. J. 23 (2) (2020) 405–420.
[23] S.A. Rizvi, W. Ali, Mathematical modelling and optimization of surface roughness and material removal rate during the machining of AISI 1040 steel, Acad. J. Manufac. Eng. 19 (3) (2021) 50–57.
[24] M. Shehab, L. Abualigah, H. Al Hamad, H. Alabool, M. Alshinwan, A. M. Khasawneh, Moth–flame optimization algorithm: variants and applications, Neur. Comput. Appl. 32 (14) (2020) 9859–9884.
[25] C.Y. Lee, T.A. Le, Y.C. Chen, S.C. Hsu, Application of salp swarm algorithm and extended repository feature selection method in bearing fault diagnosis, Mathematics 12 (11) (2024) 1718.